Waste inventory for a circular solar cell production value chain

Public initial waste inventory

Gaute Stokkan, Yijiang Xu and Martin Bellmann (SINTEF)

This project has received funding from the European Union's Horizon 2020 research and innovation programme under grant agreement number 958365.

CONTENTS

1 Introduction ... 3
2 Theory ... 3
2.1 Solar cell value chain ... 3
2.2 Hot-zone graphite and silica ... 4
2.3 Silicon kerf ... 4
3 Materials and methods ... 5
3.1 Materials ... 5
3.2 Characterization methods ... 6
4 Results ... 6
4.1 Silicon kerf ... 6
4.2 Graphite ... 10
4.3 Silica ... 11
5 Discussion ... 12
5.1 Silicon kerf ... 12
5.2 Graphite ... 13
5.3 Silica ... 13
6 Conclusion ... 14

This project has received funding from the European Union's Horizon 2020 research and innovation programme under grant agreement number 958365.

1 Introduction

A carbon neutral energy supply will rely heavily on the use of solar energy in different forms. Photovoltaics (PV), i.e. the generation of electricity from solar cells will be a cornerstone, and the production and deployment of solar panels have soared during the past 20 years, and PV now accounts for 60% of the global increase in renewable energy, according to IEA[1]. The production of solar cells is both a mature and immature industry at the same time: It is mature since robust industrial techniques exist that supply energy in amounts already comparable to traditional energy sources: nuclear, hydropower and fossil energy. It is immature because the development has occurred so fast that optimized routes for efficient resource handling need to be developed. During the production of solar panels large resource flows are generated, which currently largely end up as waste. Here to the challenge in re-use is connected to the material properties: The composition, purity and morphology will determine how the current waste should be processed in order to realize the value potential. We have therefore performed a waste inventory for three important material flows occurring from silicon-ingot and wafer manufacturing in the PV production value chain: Si kerf from sawing of wafers, silica from crucibles used in crystal pulling and graphite from crystal growth furnaces. Utilising the circular potential of these waste products, 9.6 Mt of silicon, 1.2 Mt of silica and 0.6 Mt of graphite could be unlocked by 2050 as secondary raw materials.

2 Theory

2.1 Solar cell value chain

The solar cell value chain starts with carbothermic reduction of natural quartz to produce silicon, which is later purified to achieve a purity level of at least 99.9999% (6N), usually by the so-called Siemens process where silicon is reacted with HCl to produce silane gas (SiH_4), fractionally distilled and re-deposited in hot bell-reactors. The silicon feedstock is of high-purity but poly-crystalline and is made into single crystalline cylindrical ingots in the so-called Czochralski process (CZ), where silicon is melted in a fused quartz crucible, from which the ingot is pulled out slowly. The ingot is cut by a diamond band saw into suitable lengths from which edge segments are removed, producing square blocks. The blocks are cut into wafers using Fixed Abrasive Sawing (FAS): the friction between diamonds attached to a steel wire carves away the silicon, leaving thin wafers (~160 µm) which are subsequently processed to solar cells through several different chemical treatments. There are different cell architectures requiring different steps, and since these are not part of the material flow chains investigated here, they will not be described in detail.

[1] IEA: Renewable energy market update, May 2022

This project has received funding from the European Union's Horizon 2020 research and innovation programme under grant agreement number 958365.

2.2 Hot-zone graphite and silica

High purity isostatic graphite is used for high temperature parts of the silicon melting and crystallisation furnace. Graphite parts used in the hottest sections of the furnace have a lifetime of only about a few months. Then the structural integrity has decreased to a level that process failure becomes too pronounced.

The crucible where silicon is melted and kept molten during the ingot production is made of amorphous silica. The fused silica crucibles for single crystal CZ ingot growth consist of fused quartz in two layers made of different quality sands: A thick outer layer with bubbles for structural integrity and a bubble-free inner layer to reduce contamination of the melt by dissolution or release of particles. During the CZ-process, the silica goes through a phase change, particularly on the inner surface, forming cristobalite. Homogeneous formation of cristobalite is aided by a barium mineralizer, either as a coating on the crucible surface, as doping in the crucible inner layer or added to the melt. After several runs, many bubbles form and grow in the bubble free layer, which will be detrimental for growing ingot. The crucible breaks after the cool-down and cannot be reused.

The furnace hot zone is a chemical system containing Si, C and O, seeking to achieve equilibrium through chemical reactions between the parts. Thus, the materials will be contaminated by compounds containing the other elements, as described in *Table 1*. The silicon is doped, usually by P, B or Ga, which is also transported to the other materials.

2.3 Silicon kerf

The silica crucible dissolves slowly into the silicon melt, and impurities from the crucible partly end up in the ingot along with the doping elements and the trace amounts of impurities in the feedstock. The Si kerf is the by-product of the FAS producing wafers, and the kerf contains the same impurities as the ingot, in addition to impurity contamination during the sawing process. An electroplated nickel coating is used to attach the diamonds to the cutting steel wire. The wire is strung up in a web and moved at high speed. Silicon bricks which are mounted to a beam are fed into the moving wire web while being bathed in a water-based cutting fluid. Depending on the wire thickness, around 35% of the silicon is lost as Si-kerf which is dispersed in the cutting fluid. The cutting fluid and the Si-kerf are later separated through a filter press providing a liquid and a solid fraction (Si-kerf filter cake). The main impurity sources in this process are the beam material used for sawing, the adhesives bonding the silicon to the beam, the nickel coated steel wires, surfactants and additives used in the water based cutting fluid and a filtration aid to avoid blocking of the filter press. The kerf contamination is also summarized in *Table 1*.

This project has received funding from the European Union's Horizon 2020 research and innovation programme under grant agreement number 958365.

Table 1: Overview of potential contaminations sources of the waste products and their composition and impurities.

	Potential contamination source	Impurity/composition
Si-kerf	Steel wire with electroplated nickel coating and diamonds	Iron, nickel, carbon
	Wire spools	Aluminium
	Beam holding the silicon brick	Aluminium tri-hydroxide, polymethyl methacrylate (engineering plastics, acrylic glass)
	Adhesive bonding (beam/silicon brick)	Epoxy based adhesives, organic compounds
	Cutting fluid	Organic compounds, surfactants, water
	Filtration aid	Diatomaceous earth (80-90% silica, 2-4% alumina, 0.5-2% iron oxide)
	Silicon dopants and impurities	Boron, phosphorous, gallium, carbon and oxygen
Graphite	Chemical reactions	Silicon carbide, silicon, silicon dopants, silicon dioxide
Silica	Devitrification agent/coating	Barium (other alkaline-earth metals)
	Crucible impurities	Main impurity is aluminium (13-18 ppm) in HPQ sand
	Chemical reactions	Silicon pot scrap, silicon droplets

3 Materials and methods

3.1 Materials

The materials investigated are summarized in *Table 2*. The materials from Norway have been received with higher level of information about processing than those originating in Asia or of unknown origin. Most of the samples have been pre-processed by industrial methods relevant for a recycling process (drying/crushing), while the kerf is investigated both in a dry and wet state.

Table 2 Nomenclature of waste products subjected for analysis

Waste type	Origin	ID	Condition
Si-kerf filter cake	Norway	RST-ODIN-0921-Si-wet	as-filtered
Si-kerf dry (2x)	Norway	RST-ODIN-0921-Si-dry/0821-Si-dry	Dried

This project has received funding from the European Union's Horizon 2020 research and innovation programme under grant agreement number 958365.

Si-kerf dry (3x)	Asia	RST-HAN-0120-Si/MING-020-Si/SONG1-0721-Si	Dried
Si-kerf dry (2x)	n.a.	RST-1-1/2	Dried
Hot-zone graphite	Norway	RST-ODIN-C	crushed
Silica crucible scrap	Norway	RST-ODIN-Q-0921	crushed

3.2 Characterization methods

The materials are investigated by methods suitable to investigate the contamination properties identified in *Table 1*.

Inductively coupled plasma mass spectrometry (ICP-MS) is known and used for its ability to detect metals and several non-metals in liquid samples at very low concentrations. The sample is digested into suitable acids, which is ionized using the inductive coupled plasma, and the composition is analysed using the mass spectrometer.

LECO is a common name for the (actually a brand name) for *Inert Gas Fusion Analysis* and *Combustion Infrared Analysis.* The samples are reacted at high temperature, forming volatile gases which are analysed using infrared absorption. The total concentration of hydrogen, nitrogen, oxygen, carbon and sulphur contamination can be analysed.

X-ray photoelectron spectroscopy (XPS) is used to measure surface impurities, here the surface oxide on the kerf.

The water content of a sample is measured by weight loss during a heating sequence where water is evaporated until equilibrium weight is reached.

X-ray diffraction analysis (XRD) determines the crystallographic structure and phases of a material. XRD works by irradiating a material with incident X-rays and then measuring the intensities and scattering angles of the X-rays that leave the material.

Sample size and morphology is quantified by measuring particle size distribution using *laser diffraction* and specific surface area using nitrogen adsorption/desorption (Brunauer-Emmet-Teller method). Morphology is also characterized by microscopic techniques, both light microscopy and scanning electron microscopy (SEM).

4 Results

4.1 Silicon kerf

Figure 2 shows the content of common dopant elements (B, Ga and P) in different Si-kerf samples. The main impurity is P, ranging from 4 to 15 ppm, indicating that the kerf mainly origins from P-doped n-type crystals. However, B is present in not insignificant amounts in all samples,

This project has received funding from the European Union's Horizon 2020 research and innovation programme under grant agreement number 958365.

0.35 to 0.6 ppm, and Ga in more varying amounts, from 0.05 to 0.65. During the wafer sawing process crystals are processed as-incoming independent on the type of doping and it is therefore assumed that the kerf contains a mixture of dopants. The dopant elements and concentration will therefore strongly vary with the set of processed crystals.

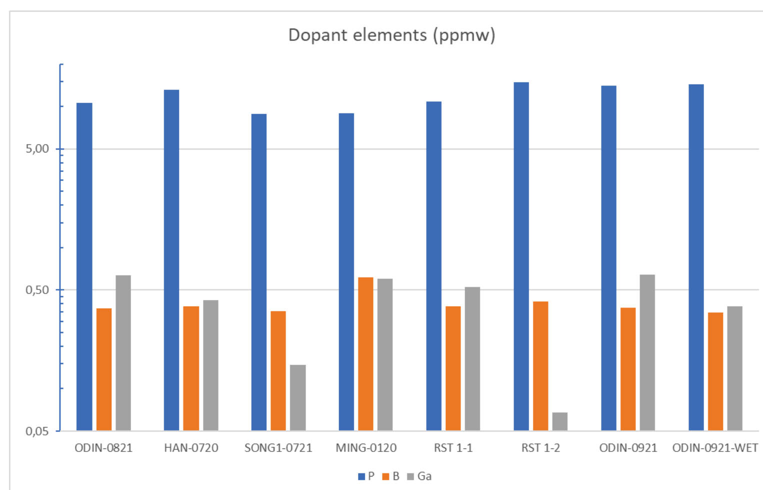

Figure 1: Content of common dopants (B, Ga and P) in different Si-kerf samples measured by ICP-MS.

Metal contamination is actually much higher than the dopant levels, due to the contamination sources in *Table 1* being primarily metallic. Concentrations of the most prominent impurities are shown in *Figure 3*. Al can reach very high levels, up to 7000 ppm in the ODIN samples, but other samples are significantly lower, notably SONG1 below 10 ppm. There is similar Ca content (500-700 ppm) in all the dry samples. The Fe contamination varies over two orders of magnitude, but one sample, MING, is significantly higher than the rest, the common level ranging between 10 and 100 ppm. Ni from the electroplated steel wire is fairly similar between the samples, between 120 and 180 ppm, while one sample, RST 1-2, of unknown origin, is significantly lower at 25 ppm.

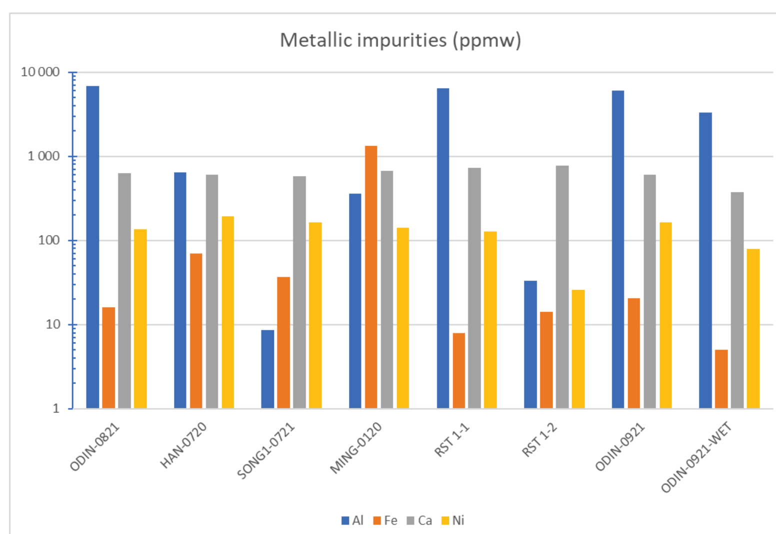

This project has received funding from the European Union's Horizon 2020 research and innovation programme under grant agreement number 958365.

Figure 2: Content of metal impurities (Al, Ca, Fe, Ni) in different Si-kerf samples measured by ICP-MS.

The carbon and oxygen content were analysed as a round robin test among three partners, and deviations were shown to be small. Average values are shown in Table 3. The typical carbon content for most of the samples is around 1-2 wt.%, while SONG1 is more than double this. The oxygen content is about 4-5 wt.%. N, S and water content of ODIN-0921 wet and dry are also shown in *Table 3*.

Table 3: Carbon and oxygen content measured by LECO.

Sample-ID (wt.%)	RST-ODIN-0921-dry	RST-ODIN-0921-wet*	RST-ODIN-0821	RST-HAN-0120	RST-MING-0120	RST-SONG1-0721	RST1-1	RST1-2
Carbon	2.0	2.4	1.8	2.0	1.0	4.4	1.8	1.5
Oxygen	4.2	4.5	5.1	4.3	4.8	5.6	4.9	3.9
Nitrogen	0.07	0.05						
Sulphur	0.10	0.15						
Water (wt.%)	0.7	47.2						

** The wet sample has been dried before analysis. And the results shown here are the carbon and oxygen content in the sample after drying.*

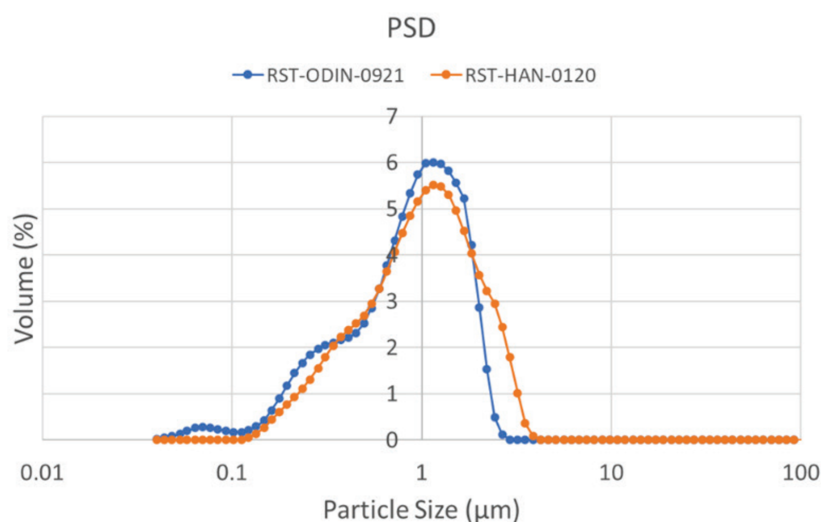

Figure 4: Particle size distribution of 2 Si-kerf samples (RST-ODIN-0921 and RST-HAN-0120).

This project has received funding from the European Union's Horizon 2020 research and innovation programme under grant agreement number 958365.

Figure 4 shows the particle size distribution (PSD) of two representative Si kerf samples from Norway and Asia. The corresponding surface area 22 m^2/g and 20 m^2/g for ODIN-0921 and for HAN-0120.

Figure 5 shows an SEM image of RST-ODIN-0921-dry Si-kerf sample. It is seen that the Si-kerf consists of ribbon-like, irregular shaped angular particles, agglomerates, and nano-sized particles. The ribbon shaped particles are up to around 4 µm long. XRD confirms crystalline silicon phase, but a broad peak around 2θ=12.5° indicates the presence of an amorphous phase.

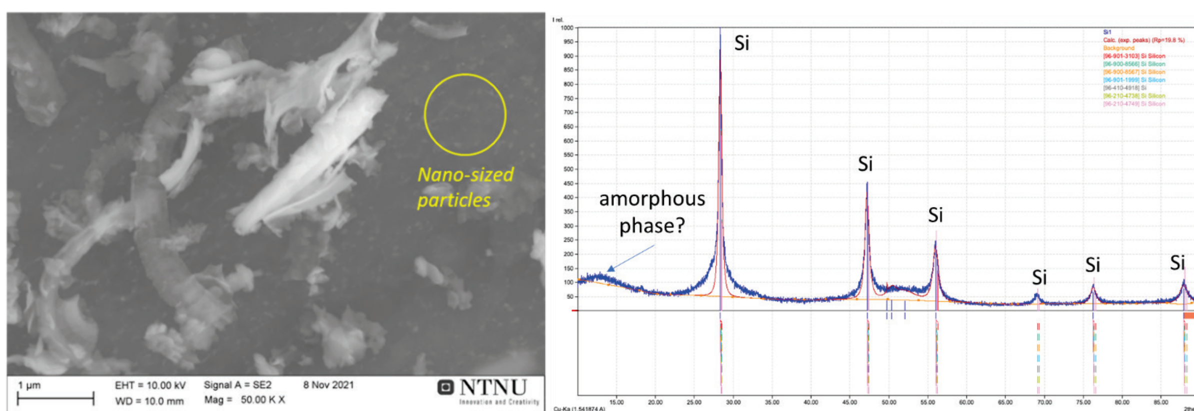

Figure 3: Left: SEM images of RST-ODIN-0921-dry Si-kerf sample. Right: XRD spectrum of the same sample.

The surface contamination observed by XPS for RST-ODIN-0921-dry Si-kerf sample is shown in Figure 6. Figure 6 a) is a survey spectra in an area 700 um x 300 um. The main elements detected are carbon, silicon and oxygen. Small amount of aluminium is also identified, while indium is from the substrate but not from the sample. Figure 6 b) is a detail spectra of silicon. The Si and SiO_2 contributions can be seen clearly. Based on this spectrum, the thickness of SiO_2 layer was estimated to be around 1-2 nm. Figure 6 c) is a detail spectra of carbon, and there is considerable amount of carbon in the form of organic carbon. Figure 6 d) is a detail spectra of oxygen. Both organic oxygen and other oxides (mainly SiO_2) exist in the samples.

This project has received funding from the European Union's Horizon 2020 research and innovation programme under grant agreement number 958365.

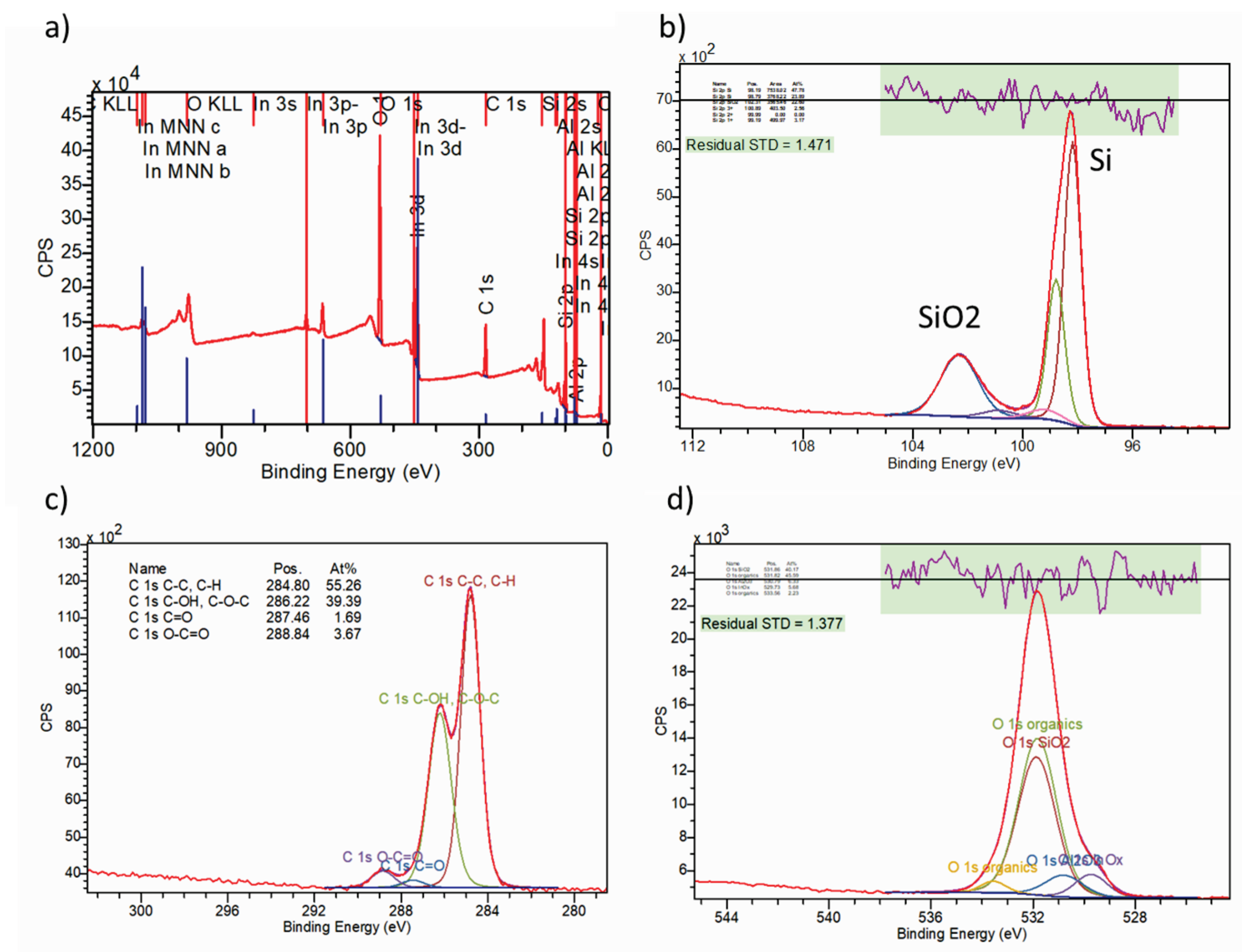

Figure 4: X-ray photoelectron spectroscopy(XPS) analysis of the RST-ODIN-0921-dry Si-kerf sample.

4.2 Graphite

Graphite samples have been sorted according to their visual appearance: 1: “clean” samples, 2: yellow surface, 3: silver-grey surface, 4: silver-grey with droplet. Surface phase composition was measured by XRD on samples of type 2, 3 and 4. Type 2 show crystalline SiO_2 and SiC phases, while type 3 and 4 show SiC and Si phases. The visual appearance of type 2 graphite is shown in *Figure 8* along with a SEM micrograph. The two different regions correspond to SiC (large grained structure) and SiO_2 (small grained). The silicon detected on graphite type 3 are in the form of small particles on the SiC surface. The silicon on graphite type 4 forms a continuous layer with SiC crystals forming islands. Ash content was measured for all four types: Type 1 is significantly cleaner than the other types with 0.16%, vs. respectively 5.2%, 4.5% and 4.1% for the others.

The ash from two randomly selected samplings of crushed graphite (without reference to the types above) was analysed by ICP-MS. The results are shown in *Table 4*; Si is the most prominent impurity, followed by Fe, with Ni and Co quite low.

This project has received funding from the European Union’s Horizon 2020 research and innovation programme under grant agreement number 958365.

Table 4: Impurity content in graphite bulk material (recalculated)

	$Si_{wt\%}$	$Ca_{wt\%}$	$Al_{wt\%}$	$Fe_{wt\%}$	Cr_{ppmw}	Ni_{ppmw}	Co_{ppmw}	B_{ppmw}	P_{ppmw}	Ga_{ppmw}
#1	0.485	0.0048	0.0062	0.0326	38.4	3.00	0.14	0.46	4.30	0.02
#2	1.9754	0.0124	0.0340	0.0780	27.62	12.64	0.41	0.79	5.90	0.11

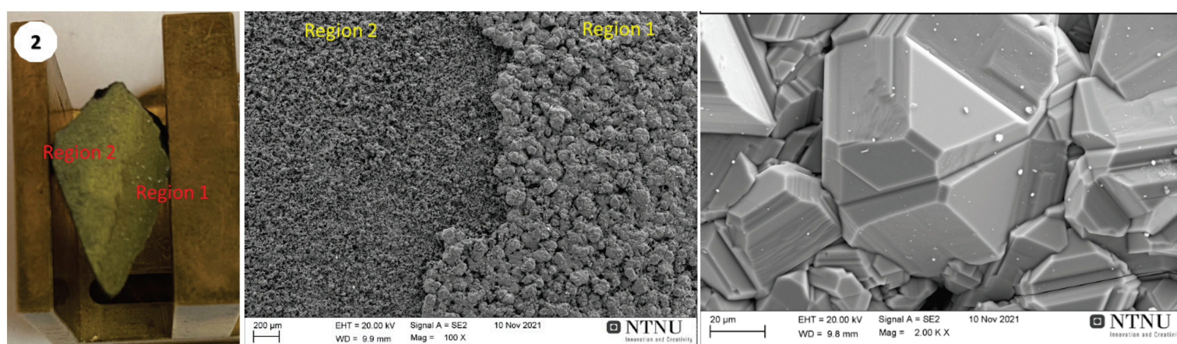

Figure 5: **a)** *Low magnification SEM micrograph of graphite type 2 surface, the left is a photo of the corresponding sample, where there are 2 regions with different colour and thickness. Region 1 is SiC and region 2 is SiO_2. b) SEM micrograph of SiC crystals on surface of graphite type 3, with small silicon particles on the surface.*

4.3 Silica

Silica samples were sorted according to visual inspection into the following categories: Type 1: white inner and outer surface, type 2: small yellow and black dots at the inner surface, type 3: yellow dots and extended regions on the outer surface, type 4: silver-like particles on the non-flat inner surface.

The impurity content determined by ICP-MS is shown in Table 5. The highest impurity is Ca, which is much higher than the typical amount in the new crucibles for CZ process. Co is around 21.4 ppm, which is also higher than the typical value (<0.01 ppm), which could be a result from contamination during the milling process. Similar for Fe, the samples could have been contaminated during crushing process if steel tools have been used. Comparing the 4 samples, it can be seen that type 3 has much higher Al content than the other 3, which are almost the same as in the original quartz sand and new crucible. Sample type 2 has low Fe and low P compared to the other.

Table 5: Impurity content (ICP-MS) in the 4 categorised silica samples. All values in ppmw

#	Na	Al	P	Ca	Ti	Fe	Co	Ba	B
1	11.8	16.7	1.4	518.4	6.7	10.1	25.2	2.1	0.2

This project has received funding from the European Union's Horizon 2020 research and innovation programme under grant agreement number 958365.

2	13.4	10.6	0.6	433.7	6.2	2.4	24.0	1.4	0.6
3	30.1	135.4	1.5	403.5	2.7	37.0	17.4	1.1	<0.2
4	25.0	7.5	1.1	431.2	2.0	26.6	19.0	1.1	<0.2

Figure 9 shows the XRD results of powder sample of silica type 4, which is similar to the pattern obtained for the other three types. A sharp cristobalite peak is observed, which is the only crystalline phase. There is a flat bump at $2\theta=23^{o}$, which corresponds to the amorphous silica phase.

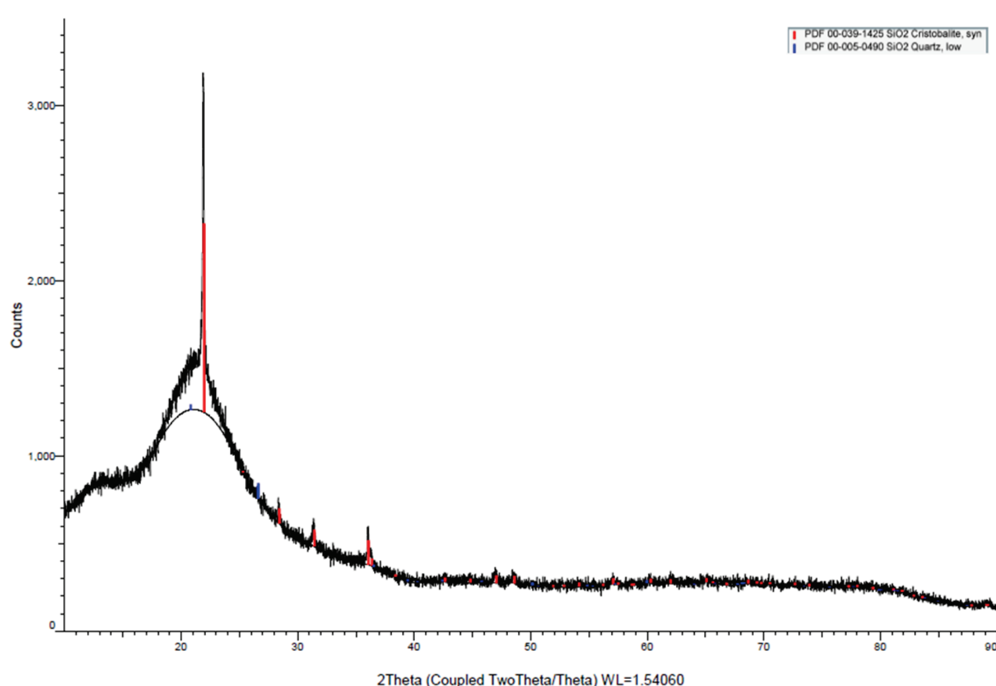

Figure 6: Powder XRD results of silica sample type 4. Same pattern was obtained for the other 3 sample types as well.

5 Discussion

5.1 Silicon kerf

For recycling of Si kerf back into the PV value chain as new feedstock, the contamination level is an important parameter. All dopants (P, B, Ga) exist in all samples. For a recycling process of kerf back into the PV chain, choice of kerf with the same dopant as in the new product will be helpful, but not sufficient. Al is also a doping element, although not used intentionally, which comes from the cutting process. In order to avoid resistivity problems in the new material connected to this, the cutting process could be adapted, particularly the choice of beam material. The variations between the samples shows that this is a possible measure. Besides, a further refining process

This project has received funding from the European Union's Horizon 2020 research and innovation programme under grant agreement number 958365.

could also reduce the impurity level to the required amount, which is under development in the ICARUS project.

Recombination active elements like Fe and Ni come from the cutting wire itself. While Ni contamination varies only slightly, this is not the case for Fe. We have not been able to correlate the variations to process parameters due to the unknown origin of some of the samples, but different levels could result from different degrees of wire wear because of different processing conditions. For the alkaline metals Ca is the most prominent, in the order of 100 ppmw. A potential source of Ca might be the water from the cutting fluid which is based on sweet water from a lake.

Use of Si-kerf in new products implies various processing such as drying, cleaning, refining, briquetting, pelletizing. The processability will depend on morphology and surface conditions. It is seen that some differences exist between materials in terms of particle size and surface area, although the differences are not very large. The microscopic particle morphology does not vary much between the samples, being characteristic of the fixed abrasive sawing technique, which on the other hand is very different from the morphology of the loose abrasive sawing technique used earlier. Surface oxygen varies only slightly, which is reasonable if the main source is the surface oxide being formed in contact with water or air. The surface oxide forms a protective layer preventing further oxidation, but also raise challenges for recycling in some cases. Carbon varies slightly, which could be a result of how successful the removal of the organic component of the cutting fluid has been during the post-processing. Other main contributors are organic compounds in the adhesives, in the beam and in filtration aid as well as the diamonds attached to the steel wire.

5.2 Graphite

The visual inspection appears to be a good sorting criterion for surface contamination of Si, SiO_2 and SiC. Several chemical reactions involving the elements Si, C and O occur in the furnace ambient, and the balance depends on the local temperature as well as gas flows. This leads to different degrees and types of surface contamination. Elemental silicon could be the result of splashing during recharge of Si feedstock into the crucible.

The ash content is a factor 30 higher in type 2,3 and 4 compared to type 1, which again is a factor 8 higher than pure, unused graphite. The sampling routine for ICP-MS did not distinguish between type. The scattering results show that the sampling routine should be improved. The generally low levels of Ni and Co are promising for typical graphite uses.

5.3 Silica

The differences in impurity concentration between the types are not significant, except type 3 which has an order of magnitude higher Al concentration and also much higher Fe concentration. The presence of cristobalite is confirmed for all samples.

This project has received funding from the European Union's Horizon 2020 research and innovation programme under grant agreement number 958365.

6 Conclusion

The main doping element corresponds to the added doping (in this case P), but other dopants are also present. Certain metallic impurities are present in higher concentrations than the dopants, notably Fe, Ni and Al (in the order of 1000 ppmw). The contamination occurs during the sawing process, and the main contamination sources are the Ni-electroplated steel wire and the beam holding the silicon brick during wafer sawing. Again, specific concentration levels will depend on the sawing technology used by different manufacturers.

For the alkaline metals Ca is the most prominent revealed in Si-kerf (order of 100 ppmw) probably from the water in the cutting fluid. C and O light elements are in the order of 10 000 ppmw, resulting from oxidation of the kerf particles and organic residues from the cutting process. The thickness of the oxide layer was revealed to be in the order of 1-2 nm. The core of the particle consists mainly of crystalline silicon. However, there are some indications that an amorphous phase could be present as well. The Si-kerf particle size is in the order of 0.3 to 2.4 µm. The particle size and its distribution will depend on the diameter of the used sawing wire. Si-kerf has a relative high surface area. 1 g of Si-kerf comprises a surface area of around 20 m^2.

Graphite contains mainly Si and surface infiltrations of SiC and SiO_2 originating from the chemical reactions inside the furnace hot zone. Silicon droplets are present as well, which can occur through silicon recharge operations (splashing). Other detected impurities, but at much lower levels (1-800 ppmw), are Ca, Al, Fe, Cr, Ni, Co, B, P and Ga.

Silica is mainly present in the form of amorphous silica and crystalline cristobalite. In type 4, it can contain silicon. Ca has the highest level (~500 ppmw) among other impurities. Other impurities like Na, Al, P, Ti, Fe, Co, Ba and B are also present but at much lower levels (1-40 ppmw).

This project has received funding from the European Union's Horizon 2020 research and innovation programme under grant agreement number 958365.